Semnan University

Progress in Engineering Thermodynamics and Kinetics Journal

Journal homepage: https://jpetk.semnan.ac.ir/

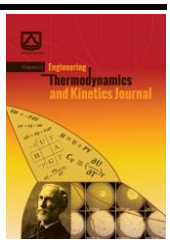

Research Article

The Kinetic Modeling of Methane Hydrate Growth by Differential Scanning Calorimetry Measurements and Molecular Dynamic Simulations

Parisa Naeiji *

School of Chemical & Bioprocess Engineering, University College Dublin, Belfield, Dublin 4, Ireland

ARTICLE INFO

Article history:

Received: 202*-**-**

Revised: 202*-**-**

Accepted: 202*-**-**

Keywords:

Differential Scanning Calorimetry;

Molecular Dynamic Simulation;

Growth Kinetics;

Non-Equilibrium Thermodynamics;

Gas Hydrate.

ABSTRACT

The formation kinetics of methane hydrate were examined using differential scanning calorimetry (DSC) and molecular dynamics (MD) simulations. A kinetic model was established based on the principles of irreversible and non-equilibrium thermodynamics and the concept of the thermodynamic natural path. This model employed affinity as a thermodynamic function, driving the hydrate formation process. It accurately predicted methane hydrate growth from both experimental and simulation data, demonstrating that hydrate formation follows a natural path. This model includes two parameters with distinct dependencies. One parameter, n, remained nearly constant, with experimental results averaging -6.8 and simulation data ranging from -1.05 to 1.46. The other parameter, k, is influenced by operational conditions and serves as a kinetic index. The value of k changed with variations in temperature, pressure, and additive concentration, increasing by 10 to 100 times with higher system pressure and by 2 to 3 orders of magnitude with the addition of tetrahydrofuran.

1. Introduction

Gas hydrates are crystalline solids formed by trapping small gas molecules, like methane, or polar molecules, such as tetrahydrofuran (THF), within water cavities composed of hydrogen-bonded water molecules [1,2]. Methane hydrate reservoirs on the deep ocean floor are estimated

* **Corresponding author.**
E-mail address: parisa.naeiji@ucd.ie

Cite this article as:
Naeiji, P. (2025). The kinetic modeling of methane hydrate growth by differential scanning calorimetry measurements and molecular dynamic simulations. *Progress in Engineering Thermodynamics and Kinetics*, 1. (3), pp. 243-260.
https://doi.org/10.22075/jpetk.2025.24839.1003

to contain about 6.4 trillion tonnes of methane [3], representing a significant potential energy resource. However, these hydrates can pose challenges for the petroleum industry by occluding gas transport pipelines. Therefore, improving our understanding of these compounds could offer new insights into previous experimental and theoretical data.

Research has focused on understanding the fundamental mechanisms of nucleation, growth, and dissociation of gas hydrates. Continued investigation into these processes remains critical for advancing strategies in methane hydrate exploration and exploitation [4-8]. Prof. Bishnoi's group, a pioneering force in the field, has been at the forefront of macroscopic kinetics studies of hydrate growth and decomposition since the early 1990s, pioneering the kinetic modeling of gas hydrates [9-11]. Subsequent research has increasingly integrated time-dependent measurements across macroscopic, mesoscopic, and molecular scales, leveraging advanced experimental and computational techniques developed over the past two decades.

Differential scanning calorimetry (DSC) is one of the most widely used methods for measuring the thermal properties associated with gas hydrate formation and dissociation [12,13]. Researchers such as McNamee and Dalmazzone et al. have demonstrated that DSC is an effective tool for evaluating hydrate formation kinetics [14,15]. For instance, Dalmazzone et al. utilized DSC data to develop a model based on crystal growth theory, which quantifies the hydrate formation rate over time [16].

In addition to macroscopic measurements and kinetic modeling, understanding the molecular mechanisms of hydrate formation is crucial for explaining its various properties. Molecular dynamics (MD) simulations are a powerful tool for elucidating crystal growth mechanisms [17-22]. Nada postulated that gas hydrate growth involves transferring gas molecules from the gas phase through the liquid phase to the liquid/clathrate interface, followed by the organization of water molecules around the gas molecules at the interface [23]. These stages are key factors in the hydrate growth rate and should be incorporated into kinetic models. Several kinetic models of gas hydrate formation and decomposition have been based on molecular simulation data. For example, Tung et al. developed a simple adsorption-diffusion model to predict methane hydrate growth by considering methane mass transport in the bulk phase and its adsorption by water cages in the growing layer [24].

This work aims to provide a straightforward and practical approach for studying methane hydrate growth kinetics at both macroscopic and molecular levels. We utilized high-pressure DSC and molecular dynamics simulations to acquire data on methane hydrate growth kinetics and applied a model grounded in non-equilibrium thermodynamics and the concept of the thermodynamic natural path for kinetic modeling.

2. Methods

2.1. Experimental

Solutions were prepared using freshly deionized distilled water, sodium dodecyl sulfate (SDS), and tetrahydrofuran (THF; 99.5%, Merck). The experiments were carried out using a high-pressure differential scanning calorimeter (DSC) equipped with two cylindrical stainless-steel cells, each with an outer diameter of 0.4 cm, a length of 9 cm, and an internal volume of approximately 1.1 cm^3. A copper segment, comprising three rectangular cubic sub-segments, was designed to hold the cells, two platinum thermometers (Pt100), and peltiers (4 cm × 4 cm) for cooling and heating. The cells, which could withstand a maximum pressure of 20 MPa with a deviation of ±0.05 MPa, were positioned in the central segment. Each cell was equipped with thermometers placed underneath, offering accuracy of ±0.1 °C and precision of ±0.01 °C. Heat dissipation from the Peltier elements was managed by circulating a refrigerant fluid through the outer copper segments. The copper segment and its components were housed in an insulated plexiglass chamber, with temperature regulation provided by a programmable controller. A schematic of the experimental setup is illustrated in Fig. 1.

For the testing procedure, a sample of 0.25 ± 0.025 ml of the solution was injected into a pre-evacuated cell. The gas pressure was then adjusted and maintained at a constant level throughout the process. Both the sample and an empty reference cell were placed in the respective cavities of the central copper segment. The temperature was ramped down from 15 to -15 °C at a rate of 0.5 °C/min. Each experiment was performed in duplicate or triplicate to ensure repeatability.

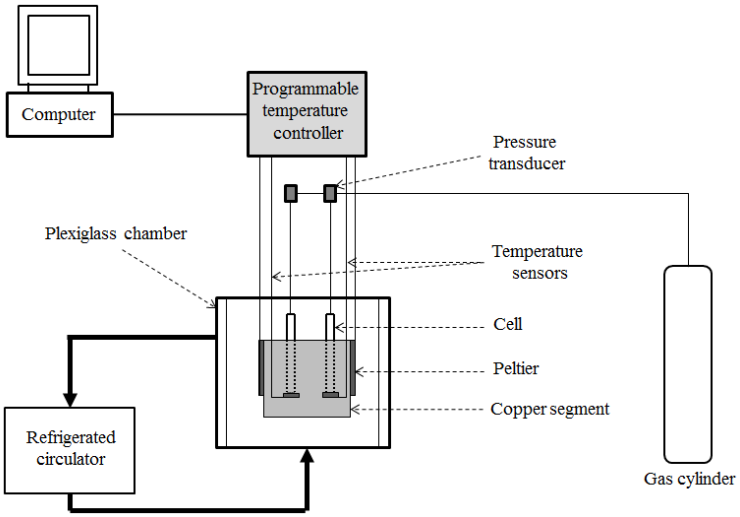

Fig. 1. Schematic diagram of the experimental apparatus of DSC.

2.2. Simulation details

All molecular dynamics simulations were conducted using the open-source software package LAMMPS [25]. The initial configuration of the simulation box, measuring 36 Å × 36 Å × 110 Å, is illustrated in Fig. 2. This setup included a 3 × 3 × 3 unit cell of structure I methane hydrate phase, flanked by two methane/water aqueous solutions. Each hydrate cavity was fully occupied by methane molecules, and each solution slab contained 1242 water molecules along with 25, 50, or 75 methane molecules, making them supersaturated methane/water solutions.

To model the intermolecular interactions of water and methane molecules, the SPC and OPLS-AA potentials were utilized, respectively [26,27]. The SHAKE algorithm was applied to constrain the bond lengths and angles of water molecules [28]. For cross-LJ parameters (ε, σ) between water and methane molecules, the standard Lorentz-Berthelot combining rules were used [29]. Long-range electrostatic interactions were computed using the Ewald method [30] with a precision of 1×10^{-4} (k-space cutoff), and all intermolecular interactions were truncated at a spherical cutoff of 11.0 Å. The force field parameters employed in the simulations are detailed in Table 1.

The equations of motion were integrated using the Verlet algorithm with a time step of 1 fs. The simulation was executed in three stages: (1) the water/methane solution phases were equilibrated using the NPT ensemble for 100 ps while keeping the hydrate phase frozen, (2) a brief 35 ps simulation was then conducted to thermalize the clathrate hydrate molecules and relieve any residual stress in the system, and (3) the simulation continued for a total duration of 10 ns under NPT conditions. The temperature was maintained between 240-270 K and the pressure between 5-25 MPa using the Nose-Hoover barostat and thermostat [31], respectively. Periodic boundary conditions (PBCs) were enforced in all directions, effectively simulating an infinite system by replicating the main cell to eliminate boundary effects, albeit with potential periodicity artifacts.

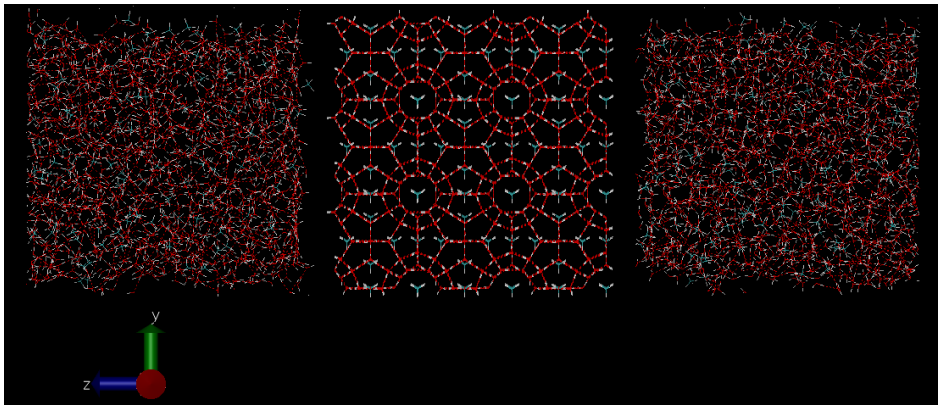

Fig. 2. The initial setup of the simulation system. Cyan, red, white spheres indicate C, O and H atoms, respectively.

Table 1. Force field parameters for water and methane [26,27].

Interaction		σ (Å)	ε (kcal/mol)	q (electrons)
H_2O	O	3.166	0.1553	-0.820
	H	0	0	0.410
		r(OH) = 1.00 Å	θ(H-O-H) = 109.47°	
CH_4	C	3.500	0.0660	-0.240
	H	2.500	0.0300	0.060
		r(CH) = 1.09 Å	θ(H-C-H) = 107.80°	

2.3. Kinetic modeling

A kinetic model was formulated to predict hydrate growth kinetics using irreversible and non-equilibrium thermodynamics along with the concept of the thermodynamic natural path [32]. When a chemical process like hydrate formation occurs in an isolated system by an amount of dξ over an infinitesimal time interval, it generates an amount of uncompensated heat, diQ, and thus creates an amount of entropy, diS. Based on this, De Donder's inequality was introduced, utilizing a new energy function termed affinity, A, for irreversible processes [33], as follows:

d_i Q=Td_i S=Adξ⟩0 (1)

This affinity equation connects the entropy generated from uncompensated heat to the irreversible chemical process occurring in nature. A positive affinity (A>0) indicates that the irreversible reaction is proceeding, while A=0 signifies that the process has reached equilibrium. Consequently, the affinity decreases as the irreversible process continues, making affinity the driving force for such processes. The rate of entropy increase or heat loss can be derived from Eq. (1):

(d_i Q)/dt=T (d_i S)/dt=A dξ/dt⟩0 (2)

The thermodynamic flow, dξ/dt, can be considered the velocity of the process or the rate of conversion, as shown below:

r=dξ/dt=kA^n (3)

Therefore, Eq. (2) can be rewritten as:

(d_i Q)/dt=T (d_i S)/dt=A dξ/dt=kA^(n+1)>0 (4)

According to Eq. (4), the rate of creation of uncompensated heat and entropy production is proportional to the (n+1)-th power of the driving force, A. This model requires two parameters, k and n, for the kinetic modeling of the gas hydrate formation process.

3. Results and discussion

3.1. Methane hydrate growth from DSC measurements

Fig. 3 displays a DSC thermogram illustrating CH4 hydrate and ice formation at a pressure of 5.2 MPa. The initial peak corresponds to CH4 hydrate formation, as indicated by a significant pressure drop at around 5.5°C. The subsequent peak, near -14°C, is associated with ice formation from un-hydrated water and was excluded from further analysis.

From the right side of Fig. 3, it is evident that once hydrate formation occurs, the heat of formation is released, causing a sudden increase in heat flow to a certain value (marked as "A" in Fig. 3). Region A signifies the rapid initial growth phase where water molecules convert to gas hydrates, releasing substantial methane hydrate formation heat. When the hydrate formation rate equals that of the cooling system, the heat flow stabilizes at the peak, indicating a metastable state. This is because the heat generated by hydrate formation is not significantly higher than the cooling capacity, leading to a gradual decrease in heat flow until it returns to baseline (marked as "B" in Fig. 3). Thus, the initial step of the process (Region A) can control gas hydrate growth and is evaluated in this study.

Fig. 4 shows the heat flow over time for CH4 hydrate formation in an SDS aqueous solution with and without THF at system pressures ranging from 4.9 to 5.5 MPa. A small amount of SDS, an anionic surfactant, was added to enhance the gas/solution interface and improve CH4 diffusion into the solution. As seen in Fig. 4, both the heat flow rate and peak height increase with rising pressure. Higher pressure results in more nucleation sites with faster kinetics, accelerating growth [2]. The presence of THF also boosts the heat flow rate and peak height. Literature confirms that THF promotes gas hydrates by altering the clathrate hydrate structure [34-38]. Zhang et al. noted that adding 6 mol% THF to water significantly lowers CH4 hydrate formation pressure by forming structure II hydrate [36]. Raman measurements revealed that CH4 molecules are trapped in the small 512 cages of sII hydrate formed by THF, while the larger 51264 cages are mostly occupied by THF molecules [37]. This additive shifts the hydrate phase boundary to lower pressures and higher temperatures, increasing the driving force for hydrate nucleation [38]. Consequently, THF is recognized as an effective promoter of gas hydrate formation kinetics.

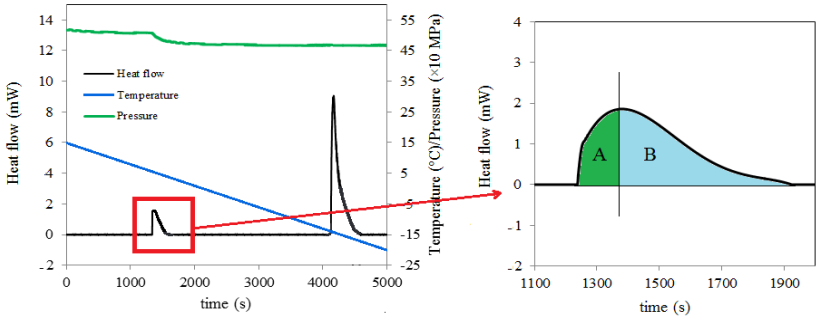

Fig. 3. DSC curve of CH_4 hydrate formation at 5.2 MPa.

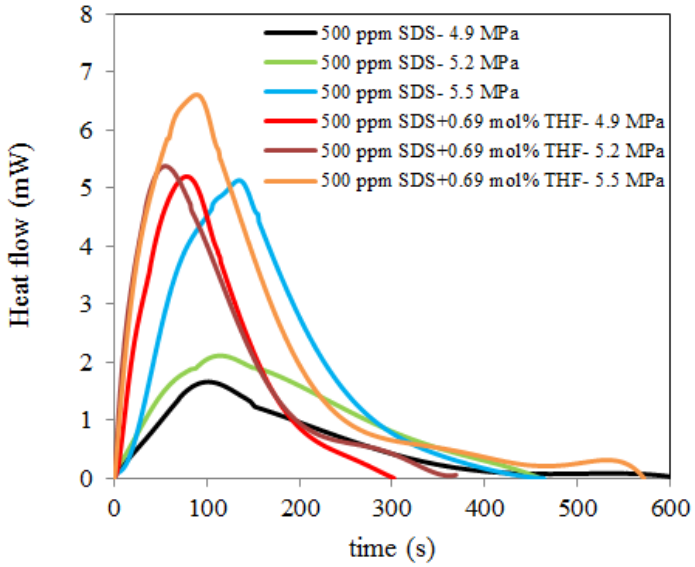

Fig. 4. DSC curve of CH_4 hydrate formation at different pressures in the presence of SDS and THF.

To determine the model parameters k and n from Eq. (3), the extent of the process ξ and the affinity A must be calculated. The extent of the process can be found by dividing the peak area of the heat flow versus time into infinitesimal segments and then calculating the ratio of the accumulated area over time to the total peak area. Fig. 5 shows the extent of the process over time for CH4 hydrate formation, displaying an S-shaped curve similar to a sigmoid growth pattern [39]. The initial portion of hydrate formation corresponds to an exponential growth rate, as illustrated in Fig. 5. Once the extent of the process is calculated, the affinity can be determined using Eq. (4):

$$A=((d\_i\ Q)/dt)/(d\xi/dt) \quad (5)$$

Fig. 5 also illustrates the affinity over time for CH4 hydrate formation at 5.2 MPa. The affinity of hydrate formation is positive (A>0) before equilibrium and zero (A=0) at equilibrium. As the process moves towards equilibrium, the affinity decreases towards zero, indicating the decay path of the affinity. Initially, at the beginning of CH4 hydrate formation, the affinity is very high but decreases as the process progresses, stabilizing at a constant value corresponding to the peak of heat flow. Subsequently, the affinity decreases further until it reaches zero. This observation indicates that as hydrate formation progresses, the diffusion of methane into the aqueous phase is impeded. The solid hydrate phase progressively covers the methane/solution interface, acting as a mass transfer barrier that hinders further growth.

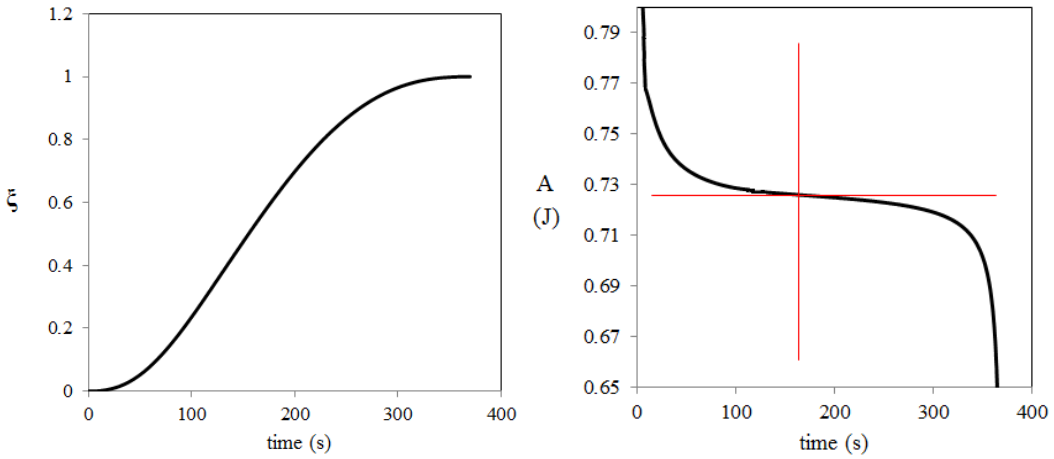

Fig. 5. The extent of process and the affinity versus time for methane hydrate formation at 5.2 MPa.

After calculating the extent of the process and the affinity for the initial stage, the two model parameters can be determined using the logarithmic form of Eq. (3):

$$ln\left(\frac{d\zeta}{dt}\right) = ln\, k + n\, ln\, A \qquad (6)$$

The results for the model parameters n and k are presented in Fig. 6 and Table 2. The parameter n was estimated to be approximately -6.8 based on the regression analysis of all experimental data. However, the parameter k did not converge to a constant value and appeared to vary with experimental conditions. As shown in Table 2, k increased by about 10-100 times with rising system pressure and by more than 2-3 orders of magnitude with the addition of THF to the solution. Therefore, k was identified as a kinetic parameter of the model, serving as a criterion for studying the kinetics of hydrate formation.

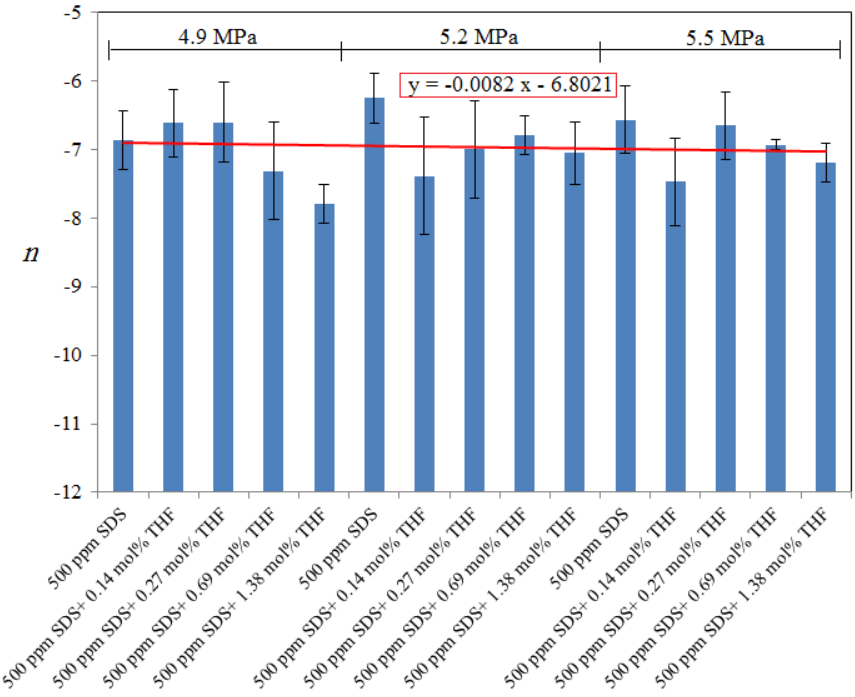

Fig. 6. The model parameter, *n*, for methane hydrate formation in the presence of SDS and THF.

Table 2. The model parameter, *k*, for methane hydrate formation in the presence of SDS and THF.

P	SDS (ppm)	THF (mol%)	*k*
55	500		4.123E-08
		0.14	7.193E-07
		0.27	3.641E-06
		0.69	8.789E-06
		1.38	5.138E-05
52	500		5.115E-09
		0.14	1.241E-08
		0.27	4.529E-08
		0.69	5.346E-08
		1.38	1.271E-07
49	500		1.978E-10
		0.14	4.963E-10
		0.27	1.624E-09
		0.69	4.989E-09
		1.38	1.039E-08

3.2. Methane hydrate growth from MD simulation

Fig. 7 illustrates the temporal evolution of CH_4 hydrate growth during the MD simulation at 240 K and 25 MPa. Over a period of 10 ns, the hydrate phase exhibits continuous expansion, as methane molecules are encapsulated within the hydrogen-bonded water network to form stable clathrate structures. Fig. 8 shows the time dependence of the number of CH_4 molecules in layers near the hydrate/aqueous phase interfaces, which are about 12 Å thick in the *z*-direction. This data was smoothed by averaging the number of molecules over short segments of the MD trajectory. As evident in Fig. 8, the number of CH_4 molecules near the interfaces increases as the initial gas molecules in the water/CH_4 solution phase rise, which is expected. Additionally, the maximum rate of hydrate growth occurs around 2 ns, followed by stabilization with negligible fluctuations.

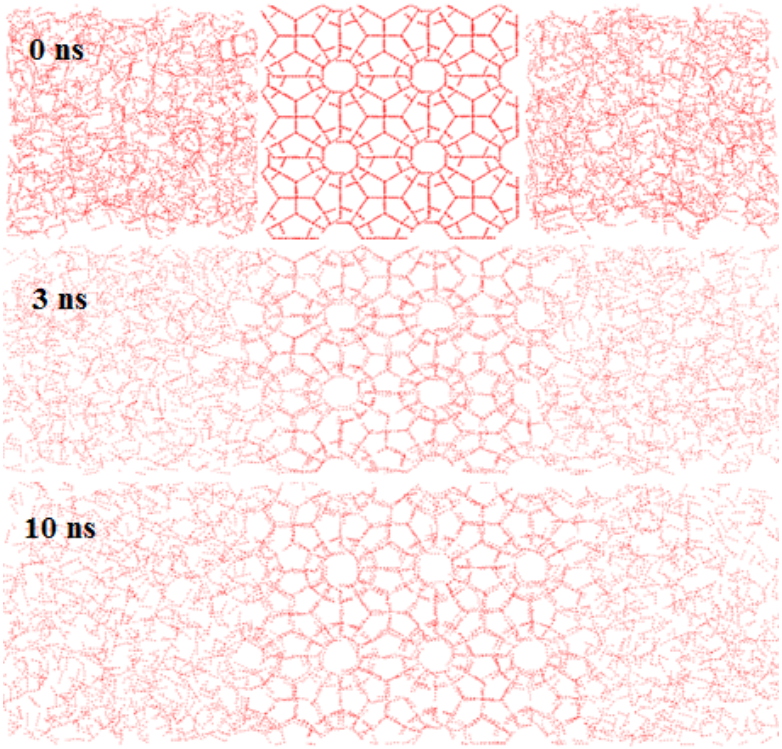

Fig. 7. The snapshots of CH_4 hydrate growth during the simulation at 240 K and 25 MPa with 50 methane molecules in the water/CH_4 solution phase.

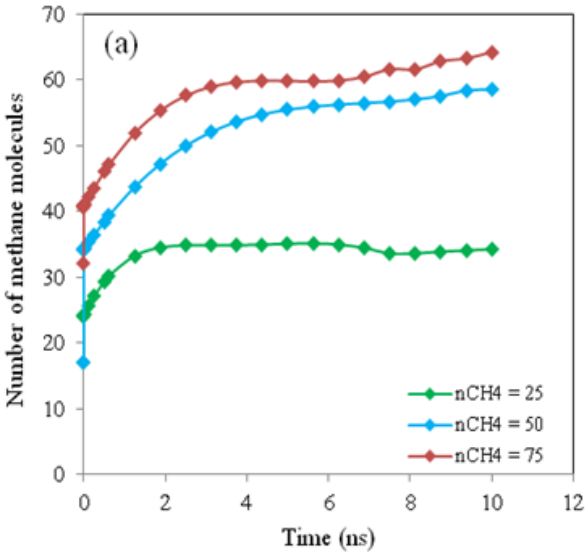

Fig. 8. The number of CH_4 molecules in the layers near the interface as a function of time at 240 K and 25 MPa with the different initial numbers of methane in the water/CH_4 solution phase.

Similar to the process for calculating the model parameters n and k from experimental data, the extent of the process ξ and the affinity A need to be determined beforehand, as follows:

$$\xi_i = \frac{N_i - N_1}{N_2 - N_1} \quad (7)$$

N_i, N_1 and N_2 represent the number of methane molecules in the layers around the liquid/solid interfaces at each moment, at the beginning and end of the simulation, respectively. The extent of the process over time for CH_4 hydrate growth is depicted on the left side of Fig. 9. It increases rapidly, approaching an exponential growth rate before stabilizing at nearly zero growth rate, indicating the end of the process. To calculate the affinity, Garfinkle's proposed equation [40] was used:

$$A_i = -RT\, ln \sum \xi_i \quad (8)$$

where R is the universal gas constant. As shown in Fig. 9, the affinity reaches its highest value when the hydrate forms. The affinity decreases sharply as the growth process continues and then slows down until equilibrium is reached, consistent with experimental observations. Subsequently, the two model parameters n and k can be determined using the logarithmic correlation of Eq. (6). The results are presented in Fig. 10 and Table 3. The values for n range from -1.46 to -1.05 under different conditions, with an estimated average of about -1.29 based on regression analysis of all simulation data. However, k did not converge to a constant value and was influenced by increasing pressure, showing a rise of more than 2-3 orders of magnitude, and also increased with decreasing temperature. The system pressure and subcooling are proportional to the driving force, leading to faster growth kinetics at higher driving forces. At higher pressures, the interfaces are enriched with gas molecules, and water molecules are more

inclined to form methane hydrate clathrates. Lower temperatures increase the solubility of gas molecules in the liquid phase and freeze the molecular motion of water molecules, making the hydrate lattices more rigid due to stronger intermolecular attractive forces. Additionally, an increase in the number of CH_4 molecules in the solution phase can raise the parameter k by about 10 times. It was expected that hydrate formation kinetics would improve as the concentration of CH_4 at the interfaces increased. Thus, k is identified as a kinetic parameter of the proposed model.

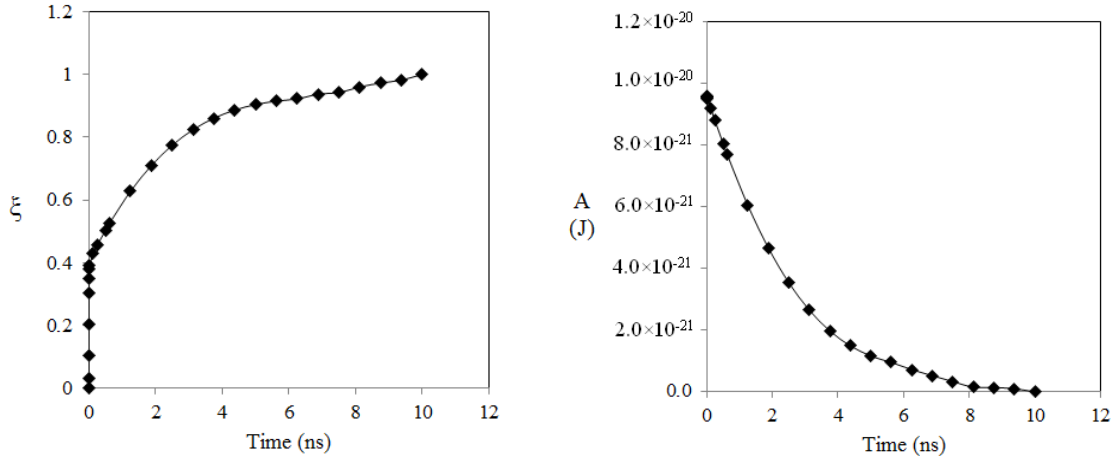

Fig. 9. The extent of the process and the affinity of hydrate growth versus time at 240 K and 25 MPa with 50 methane molecules in the aqueous solution phase.

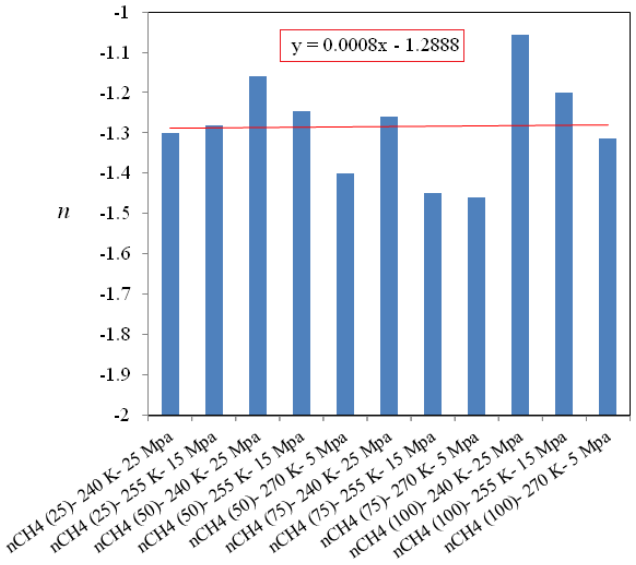

Fig. 10. The parameter of the model, n, for the CH_4 hydrate growth simulation.

Table 3. The results for the parameter of model, *k*, at different number of methane in the water/CH_4 solution phase, temperatures and pressures of the system.

n_{CH4}*	*T* (K)	*P* (MPa)	*k*
25	240	25	2.26E-32
	255	15	5.73E-33
50	240	25	8.03E-32
	255	15	6.62E-33
	270	5	1.88E-35
75	240	25	1.31E-31
	255	15	7.31E-32
	270	5	2.38E-35
100	240	25	2.49E-32
	255	15	5.43E-33
	270	5	4.04E-36

* The initial number of methane in the water/methane solution phase.

4. Conclusions

In this study, the kinetics of CH_4 hydrate formation were investigated using high-pressure DSC measurements and molecular dynamics (MD) simulations. The kinetic modeling of CH_4 hydrate growth was based on non-equilibrium thermodynamics and the concept of the thermodynamic natural path. This model involves two parameters: averaging approximately -6.8 based on experimental data, while ranging between -1.46 and -1.05 in simulation results. Conversely, the other parameter displayed variability across different operational conditions, characterizing it as a kinetic parameter. The results indicated that this parameter increased 10- to 100-fold with rising system pressure and by over 2 to 3 orders of magnitude upon the addition of THF. Discrepancies between experimental and simulation outcomes for this parameter may be attributed to the disparity between macroscopic and microscopic scales of observation.

Overall, this model represents a significant advancement compared to other kinetic models of gas hydrate growth, as it includes at least one parameter that is independent of varying conditions and can be determined both experimentally and theoretically. The proposed model effectively predicts the entire process of gas hydrate growth, as the driving force is not constant: the affinity decreases rapidly at the beginning and then more slowly until it stabilizes, even though the power of the driving force in the kinetic model remains constant.

Nomenclature

A	Affinity
k	Model parameter
n	Model parameter
n_{CH4}	Number of methane molecules

P	Pressure
q	Charge
Q	Heat of process
r	Rate of process and Distance vector
R	Universal gas constant
S	Entropy
t	Time
T	Temperature

Greek letters

σ	Cross LJ parameters
ε	Cross LJ parameter
ξ	Extent of process
θ	Angle

Subscripts

i	Denoted as irreversible

Conflicts of Interest

The author declares that there is no conflict of interest regarding the publication of this article.

References

[1] C. Giavarini, K. Hester, The Structure and Formation of Gas Hydrates, Physical Properties of Hydrates, Hydrates Seen as a Problem for the Oil and Gas Industry, Gas Hydrates, Immense Energy Potential and Environmental Challenges, Springer-Verlag, London, 2011.

[2] E.D. Sloan, C.A. Koh, Clathrate Hydrates of Natural Gases; 3rd ed., Taylor & Francis–CRC Press, Boca Raton, FL, 2008.

[3] B. Buffett, D. Archer, Global inventory of methane clathrate: sensitivity to changes in the deep ocean, Earth Planet. Sci. Lett. 227 (2004) 185-199.

[4] V. Bansal, Kinetic Study of Clathrate Hydrates, M.S. Thesis, Colorado School of Mines, Golden, CO, 1994.

[5] C.P. Ribeiro, P.L.C. Lage, Modelling of hydrate formation kinetics: State-of-the-art and future directions, Chemical Engineering Science 63 (2008) 2007-2034.

[6] R.E.T. Meindinyo, Gas Hydrate Growth Kinetics: Experimental Study Related to Effects of Heat Transfer, PhD thesis, University of Stavanger, 2017.

[7] P. Naeiji, F. Varaminian, Experimental study and kinetics modeling of gas hydrate formation of methane-ethane mixture, Journal of Non-Equilibrium Thermodynamics 38 (2013) 273-286.

[8] V.A. Vlasov, Diffusion model of gas hydrate dissociation into ice and gas: Simulation of the self-preservation effect, International Journal of Heat and Mass Transfer 102 (2016) 631-636.

[9] A. Vysniauskas, P.R. Bishnoi, Natural Gas Hydrates: Properties, Occurrence and Recovery (Cox, J.L., ed.), Butterworths, Boston, MA, 1983.

[10] A. Vysniauskas, P.R. Bishnoi, A kinetic study of methane hydrate formation, Chemical Engineering Science 38 (1983) 1061-1072.

[11] P. Englezos, N.E. Kalogerakis, P.D. Dholabhai, P.R. Bishnoi, Kinetics of formation of methane and ethane gas hydrates, Chemical Engineering Science 42 (1987) 2647-2658.

[12] M.E. Brown, Introduction to thermal analysis, Kluwer Academic Publishers, 2001.

[13] Y. Zhang, P.G. Debenedetti, R.K. Prud'homme, B.A. Pethica, Differential Scanning Calorimetry Studies of Clathrate Hydrate Formation, J. Phys. Chem. B 108 (2004) 16717-16722.

[14] K. McNamee, Evaluation of hydrate nucleation trends and kinetic hydrate inhibitor performance by high-pressure differential scanning calorimetry, Proceedings of the 7th International Conference on Gas Hydrates (ICGH 2011), Edinburgh, Scotland, United Kingdom, 2011.

[15] D. Dalmazzone, N. Hamed, C. Dalmazzone, B. Herzhaft, L. Rousseau, HP DSC investigation of the kinetiks of gas hydrate formation: application to drilling fluids, 5th International Conference on Gas Hydrates (ICGH 2005), Trondheim, Norway, 2005.

[16] D. Dalmazzone, N. Hamed, C. Dalmazzone, DSC measurements and modelling of the kinetics of methane hydrate formation in water-in-oil emulsion, Chem. Eng. Sci. 64 (2009) 2020-2026.

[17] N.J. English, J.M.D. MacElroy, Theoretical studies of the kinetics of methane hydrate crystallization in external electromagnetic fields, The Journal of Chemical Physics 120 (2004) 10247-10256.

[18] J. Vatamanu, P.G. Kusalik, Molecular Insights into the Heterogeneous Crystal Growth of sI Methane Hydrate, The Journal of Chemical Physics B 110 (2006) 15896-15904.

[19] P. Naeiji, F. Varaminian, M. Rahmati, Thermodynamic and structural properties of methane/water systems at the threshold of hydrate formation predicted by molecular dynamic simulations, Journal of Natural Gas Science and Engineering 31 (2016) 555-561.

[20] P. Naeiji, F. Varaminian, M. Rahmati, Comparison of the thermodynamic, structural and dynamical properties of methane/water and methane/water/hydrate systems using molecular dynamic simulations, Journal of Natural Gas Science and Engineering 44 (2017) 122-130.

[21] P. Naeiji, F. Varaminian, Mahmoud Rahmati, The Kinetic Modeling of Methane Hydrate Growth by using Molecular Dynamic Simulations, International Journal of Heat and Mass Transfer 142 (2019) 118356.

[22] S.E. Atakoohi, P. Naeiji, K. Peyvandi, S. Mollashahi Sanatgar, The experimental study and molecular dynamic simulation of THF hydrate growth kinetics in the presence of Arabic and Guar gum: New approaches in promotion of THF hydrate formation, Journal of Molecular Liquids 325 (2021) 115249.

[23] H. Nada, Growth mechanism of a gas clathrate hydrate from a dilute aqueous gas solution: a molecular dynamics simulation of a three-phase system, The Journal of Physical Chemistry B 110 (2006) 16526-16534.

[24] Y.T. Tung, L.J. Chen, Y.P. Chen, S.T. Lin, The growth of structure I methane hydrate from molecular dynamics simulations, The Journal of Physical Chemistry B 114 (2010) 10804–10813.

[25] P. Steve, C. Paul, T. Aidan, Large-scale atomic/molecular massively parallel simulator, Sandia National Labs, Albuquerque, 2009.

[26] H.J.C. Berendsen, J.M.P. Postma, W.F. von Gustersen, J. Hermans, Interaction models for water in relation to protein hydration. In: Pullman B, editor. Intermolecular forces, Jerusalem symposium on quantum chemistry and biochemistry. Reidel Dordrecht, 1981, 331–42.

[27] W.L. Jorgensen, D.S. Maxwell, J. Tirado-Rives, Development and testing of the OPLS all-atom force field on conformational energetics and properties of organic liquids, Journal of the American Chemical Society 118 (1996) 11225-11236.

[28] J.P. Ryckaert, G. Ciccotti, H.J.C. Berendsen, Numerical integration of the Cartesian equations of motion of a system with constraints: molecular dynamics of n-alkanes. Journal of Computational Physics 23 (1977) 327–341.

[29] H. Docherty, A. Galindo, C. Vega, E. Sanz, A potential model for methane in water describing correctly the solubility of the gas and the properties of the methane hydrate, The Journal of Chemical Physics 125 (2006) 074510.

[30] M.P. Allen, D.J. Tildesley, Computer Simulation of Liquids, Oxford, New York, 1987.

[31] W.G. Hoover, Canonical dynamics: Equilibrium phase-space distributions. Physical Review A 31 (1985) 1695.

[32] I. Prigogine, Introduction to Thermodynamics of Irreversible Processes, Wiley: New York, 1967.

[33] N. Satoh, Chemical Energy and Exergy: An Introduction to Chemical Thermodynamics for Engineers. Elsevier Science & Technology Books, 2004.

[34] D. Mech, P. Gupta, J.S. Sangwai, Kinetics of methane hydrate formation in an aqueous solution of thermodynamic promoters (THF and TBAB) with and without kinetic promoter (SDS), J. Nat. Gas Sci. Eng. 35 (2016) 1519-1534.

[35] N. Zhengfu, Z. Shixi, Z. Qin, Z. Shuangyi, C. Guangjin, Experimental and Modeling Study of Kinetics for Methane Hydrate Formation with Tetrahydrofuran as Promoter, Pet. Sci. 4 (2007) 61-65.

[36] Q. Zhang, G.-J. Chen, Q. Huang, C.-Y. Sun, X.-Q. Guo, Q.-L. Ma, Hydrate Formation Conditions of a Hydrogen + Methane Gas Mixture in Tetrahydrofuran + Water, J. Chem. Eng. Data 50 (2005) 234-236.

[37] Y.-Je Lee, T. Kawamura, Y. Yamamoto, J.-H. Yoon, Phase Equilibrium Studies of Tetrahydrofuran (THF) + CH4, THF + CO2, CH4 + CO2, and THF + CO2 + CH4 Hydrates, J. Chem. Eng. Data 57 (2012) 3543-3548.

[38] D. Mech, J.S. Sangwai, Phase Stability of Hydrates of Methane in Tetrahydrofuran Aqueous Solution and the Effect of Salt, J. Chem. Eng. Data 59 (2014) 3932-3937.

[39] A Dictionary of Zoology 1999, originally published by Oxford University Press 1999.

[40] M. Garfinkle, The thermodynamic natural path in chemical reaction kinetics, Discrete Dynamics in Nature and Society 4 (1999) 145-164.